

Origin of long-range order in a two-dimensional nonequilibrium system under laminar flows

Yuki Minami¹ and Hiroyoshi Nakano²

¹*Department of Physics, Keio University, Kanagawa 223-8522, Japan*

²*Department of Applied Physics and Physico-Informatics, Keio University, Kanagawa 223-8522, Japan*

(Dated: December 14, 2022)

We study long-range order in two dimensions where an order parameter is advected by linear laminar flows. The linear laminar flows include three classes: rotational, shear, and elongational flows. Under these flows, we analyze an ordered state of the $O(N)$ scalar model in the large- N limit. We show that the stability of the ordered state depends on the flow pattern; the shear and elongational flows stabilize but the rotational flow does not. We discuss a physical interpretation of our results based on interaction representation in quantum mechanics. The origin of the long-range order is interpreted from the advection of wavenumbers along the streamlines and its stretching effect stabilizes the order.

Introduction.— Mermin–Wagner theorem shows that long-range order (LRO) with spontaneous breaking of continuous symmetry does not occur below two dimensions in equilibrium systems [1–3]. In contrast, some nonequilibrium systems can have the LROs even in two dimensions. The celebrated example is flocking motions of active matter such as birds and bacteria [4–7]. This fact intrigues great interest in the LROs in two dimensions [8–28]. In the polar flocking of Vicsek-style models, the occurrence of the true 2D LRO has been now established [29, 30] and interests shift to their origin. Indeed, recent studies have discussed the importance of several factors such as the violations of the detailed balance, the Galilean invariance, the motility, and a non-reciprocal interaction [19, 23, 27, 28].

The nonequilibrium 2D LROs are not restricted to the active matter and are found in other systems such as an $O(N)$ scalar model under a shear flow [31–35] and a two-temperature XY model [36–38]. In the sheared model, the advection of the order parameter by the external flow stabilizes the 2D LRO. The two-temperature model has different temperatures along each space direction. In this model, the order parameter fluctuations have a long-range correlation even at a disordered state and it stabilizes the ordered state [36, 38]. Thus, several different mechanisms of the 2D nonequilibrium LROs have been found in the various systems including the active matter. However, it is unclear what is important for 2D LROs from a unified perspective and physical interpretation of the origin is still an open problem.

In hydrodynamic or field-theoretical descriptions, the Mermin–Wagner theorem is understood from a divergence of a fluctuation in the thermodynamic limit. When the continuous symmetry is spontaneously broken, a soft fluctuation generally appears [39–44]. This is called the Nambu–Goldstone (NG) mode and causes the divergence of 2D equilibrium systems: $\langle(\pi(\mathbf{x}, t))^2\rangle \sim \log L$ where $\pi(\mathbf{x}, t)$ is the NG mode fluctuation and L is the system size. Thus, the mean square of the fluctuation diverges in $L \rightarrow \infty$ and it breaks the LROs. This is called the infrared (IR) divergence and appears in various low-dimensional systems [45]. In the hydrodynamics of the polar flocking, the NG mode is the velocity fluctuation perpendicular to the flocking direction and causes the IR divergence in the linear theory [5–7]. However, it is suppressed

by the advective nonlinear interactions between the velocity and the density fluctuations, and thus the flocking order is stabilized. Furthermore, in the ordered state with the advection by the shear flow, the NG mode has the fractional dispersion relation $\omega \sim k^{2/3}$ [33]. The fractional behavior leads to the irrelevance of nonlinear interactions and suppresses the IR divergence even in the linear theory [34]. The mechanisms of the advection are different in the two systems but it suggests the importance of the advection for the 2D LRO out of equilibrium.

In this letter, we focus on a class where the order parameter is advected by stationary flows and argue the role of the advection for the 2D LRO. Even if we restrict to this class, it is unclear what effects of the advection stabilize the LRO, and under what flows the LRO occurs in general. To tackle these questions, we consider the stationary flow $\mathbf{v}(\mathbf{x})$ that is linear in the coordinate \mathbf{x} [46, 47]

$$\mathbf{v}(\mathbf{x}) = \mathcal{D} \cdot \mathbf{x} \quad \text{with} \quad \mathcal{D} = \begin{pmatrix} 0 & S + A \\ S - A & 0 \end{pmatrix}. \quad (1)$$

Here, \mathcal{D} is the coefficient matrix, and S and A are non-negative parameters characterizing the flow pattern. We call this the linear laminar flow. It includes the following three classes. For $S = A$, we have the shear flow $\mathbf{v} = (2Sy, 0)$. For $S \neq A$, the streamline is useful for understanding: $(A - S)x^2 + (S + A)y^2 = \text{const}$. For $S > A$, we have a hyperbolic flow which is called an elongational flow. For $A > S$ with $S = 0$ and $S \neq 0$, we have pure and elliptic rotational flows, respectively. Figure 1 plots the streamlines at several S and A . Onuki and Kawasaki studied the fluctuations of a critical fluid under these flows in three dimensions and showed that critical fluctuations are greatly affected [46–48].

We study an ordered state of an $O(N)$ scalar model in two dimensions where the order parameter is advected by Eq. (1). In the ordered state, the $O(N)$ symmetry is broken to $O(N - 1)$ and the corresponding NG mode breaks the order in the 2D equilibrium systems. We show that the shear and the elongational flows stabilize the ordered state but the rotational flow does not in the large- N limit. We discuss that the origin of the 2D LRO is the stretching effect of low-wavenumber fluctuations by the advection. Our study provides a different per-

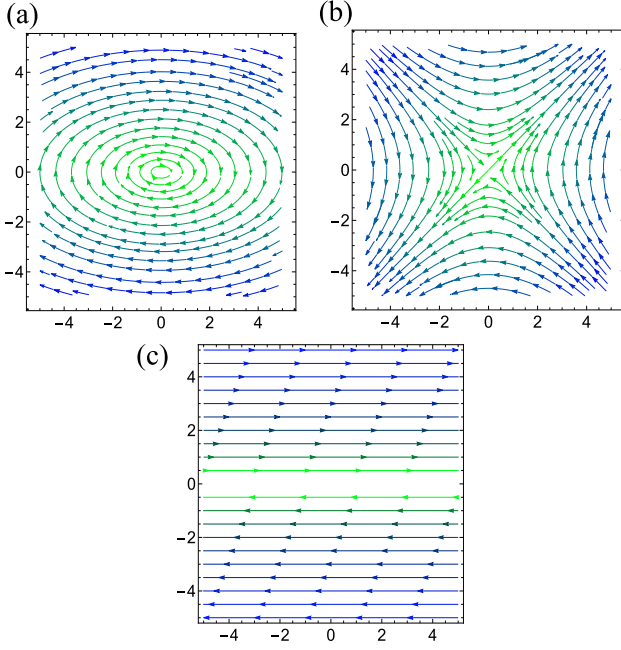


FIG. 1. Streamlines of the linear laminar flow Eq. (1) at several S and A . (a) rotational flow at $S = 0.5$ and $A = 1.0$. (b) elongational flow at $S = 1.0$ and $A = 0.0$. (c) shear flow at $S = A = 1.0$.

spective on the origin of the 2D LROs from the flocking phenomena.

Model.— We consider 1+2 dimensional $O(N)$ scalar model advected by the linear laminar flow Eq. (1)

$$\frac{\partial}{\partial t} \phi^a(t, \mathbf{x}) + (\mathcal{D} \cdot \mathbf{x}) \cdot \nabla \phi^a(t, \mathbf{x}) = -\Gamma \frac{\delta F}{\delta \phi^a} + \eta^a(t, \mathbf{x}), \quad (2)$$

where $\phi^a(t, \mathbf{x})$ is N components real scalar field and $a = 1, 2, \dots, N$, and Γ is the dissipation constant. η^a is the Gaussian noise obeying $\langle \eta^a(t, \mathbf{x}) \eta^b(t', \mathbf{y}) \rangle = 2T\Gamma \delta^{ab} \delta(t - t') \delta(\mathbf{x} - \mathbf{y})$, where T is the temperature. The free energy F is given by

$$F = \int d\mathbf{x} \sum_a \left[\frac{1}{2} (\nabla \phi^a)^2 + \frac{r}{2} (\phi^a)^2 + \frac{g}{4N} ((\phi^a)^2)^2 \right]. \quad (3)$$

This model including the advection has covariance under the $O(N)$ rotation.

Ordered state at zero temperature.— There are no fluctuations at $T = 0$ and we have the ordered state even in 2D equilibrium systems. The uniform stationary state at $T = 0$ is given by a minimum of Eq. (3) which is determined from $[r + (g/N) \sum_b (\phi^b)^2] \phi^a = 0$. For $r < 0$, we obtain the ordered state $\sum_b (\phi^b)^2 = N(-r/g) \equiv N\phi_0^2$. This only determines the radius, and then we can write the solution as $\vec{\phi}^a = (\sqrt{N}\phi_0, 0, 0, \dots, 0)$ without loss of generality. The first component breaks $O(N)$ symmetry but the remaining components have $O(N-1)$ symmetry. Consequently, the spontaneous symmetry breaking of $O(N) \rightarrow O(N-1)$ occurs. However, this ordered state is broken by fluctuations at $T > 0$ in the equilibrium system.

Fluctuations and a transition point at finite temperature.— We consider the fluctuations $\sigma(t, \mathbf{x})$ and $\pi^\alpha(t, \mathbf{x})$ from the ordered state: $\phi^a(t, \mathbf{x}) = (\sqrt{N}\bar{\phi}_R + \sigma(t, \mathbf{x}), \pi^\alpha(t, \mathbf{x}))$ where $\alpha = 2, 3, \dots, N$. Here, $\bar{\phi}_R$ is the order parameter value including the renormalization correction. From the leading-order calculation in the $1/N$ expansion, we obtain the order parameter and the mean squares of the fluctuations in the stationary state at $t \rightarrow \infty$ [49]

$$\bar{\phi}_R^2 = -\frac{1}{g} \left(r + gC_{\pi\pi} \right), \quad (4)$$

$$\langle \sigma(\mathbf{x})^2 \rangle = \int \frac{d\mathbf{k}}{(2\pi)^2} \frac{T\Gamma}{k^2 - (1/2\Gamma)\mathbf{k} \cdot \mathcal{D} \cdot \nabla_{\mathbf{k}} - 2(r + gC_{\pi\pi})}, \quad (5)$$

$$C_{\pi\pi} = \int \frac{d\mathbf{k}}{(2\pi)^2} \frac{T}{\Gamma k^2 - (1/2)\mathbf{k} \cdot \mathcal{D} \cdot \nabla_{\mathbf{k}}}, \quad (6)$$

where \mathbf{k} is the wavenumber, $\nabla_{\mathbf{k}} = \partial/\partial \mathbf{k}$ and $C_{\pi\pi} = \langle (\pi^\alpha(\mathbf{x}))^2 \rangle$. $C_{\pi\pi}$ gives the one-loop renormalization corrections from π^α to $\bar{\phi}_R$ and σ . In particular, the denominator of Eq. (5) at $\mathbf{k} \rightarrow 0$ corresponds to the renormalized “mass” of σ : $r_R \equiv -2(r + gC_{\pi\pi})$ [50]. π^α is the NG mode and thus protected from mass renormalization. We also note that the equal-time correlations have the space-translational symmetry [47] and then Eqs. (4)-(6) do not depend on \mathbf{x} .

The transition point r^* is determined from the stability of the ordered state. The stability is given as the non-negativeness of the renormalized mass $r_R \geq 0$. Namely, we have the condition for r

$$r \leq -gC_{\pi\pi} \equiv r^*. \quad (7)$$

r^* may diverge to $-\infty$ due to the IR divergence of $C_{\pi\pi}$. In fact, it logarithmically diverges in the 2D equilibrium. The negative divergence of r^* means that the ordered state does not realize in any finite r . Consequently, the IR divergence of $C_{\pi\pi}$ determines the realization of the ordered state.

IR divergence of $C_{\pi\pi}$ — To evaluate Eq. (6), we exponentiate the denominator by introducing s -integral

$$C_{\pi\pi} = T \int \frac{d\mathbf{k}}{(2\pi)^2} \int_0^\infty ds \exp \left[-s \left(\Gamma k^2 - \frac{1}{2} \mathbf{k} \cdot \mathcal{D} \cdot \nabla_{\mathbf{k}} \right) \right], \quad (8)$$

and then use the operator decomposition [46, 51]

$$\begin{aligned} & \exp \left[-s \left(\Gamma k^2 - \frac{1}{2} \mathbf{k} \cdot \mathcal{D} \cdot \nabla_{\mathbf{k}} \right) \right] \\ &= \exp \left[-\Gamma \int_0^s d\tau \mathbf{q}(\tau/2)^2 \right] \exp \left[\frac{s}{2} (\mathcal{D}^T \cdot \mathbf{k}) \cdot \nabla_{\mathbf{k}} \right], \end{aligned} \quad (9)$$

Here, $\mathbf{q}(\tau)$ is the advected wavenumber defined as

$$\mathbf{q}(\tau) \equiv \exp \left[\tau (\mathcal{D}^T \cdot \mathbf{k}) \cdot \nabla_{\mathbf{k}} \right] \cdot \mathbf{k} = e^{\tau \mathcal{D}^T} \cdot \mathbf{k}, \quad (10)$$

where the superscript T denotes transpose of a matrix. The decomposition Eq. (9) corresponds to the interaction representation of a time evolution operator in quantum mechanics with

the time variable s and the Hamiltonians $H_0 = (\mathcal{D}^T \cdot \mathbf{k}) \cdot \nabla_{\mathbf{k}}/2$ and $H_I = -\Gamma \mathbf{k}^2$ [51, 52]. Namely, we observe the diffusion H_I from the reference frame of the advection H_0 . By the decomposition, the correlation Eq. (6) turns to

$$C_{\pi\pi} = T \int \frac{d\mathbf{k}}{(2\pi)^2} \int_0^\infty ds \exp\left[-\Gamma \int_0^s d\tau \mathbf{q}(\tau/2)^2\right]. \quad (11)$$

Furthermore, by introducing $\mathcal{M}_i(\tau) \equiv e^{(\tau/2)\mathcal{D}^T}$, we write the correlation function as

$$C_{\pi\pi} = \frac{T}{4\pi^2} \int d\mathbf{k} \int_0^\infty ds \exp\left[-\mathbf{k}^T \cdot \Gamma \int_0^s d\tau \mathcal{M}_i^T \mathcal{M}_i \cdot \mathbf{k}\right], \quad (12)$$

where the subscript $i = r, e$, and s represents the rotational ($A > S$), the elongational ($S > A$), and the shear ($S = A$) flows.

To estimate the IR divergence of Eq. (12), we have to distinguish the IR and the ultraviolet (UV) divergences. Apart from the IR divergence, $C_{\pi\pi}$ has the UV divergence which comes from $|\mathbf{k}| \rightarrow \infty$ [53]. The UV divergence exists even in three-dimensional equilibrium systems and is irrelevant to our purpose. To regulate it, we introduce $e^{-\epsilon \mathbf{k}^2}$ with the infinitesimal small parameter ϵ as $C_{\pi\pi} = T \int d\mathbf{k}/(2\pi)^2 \int_0^\infty ds \exp[-\mathbf{k}^T \cdot \Gamma (\int_0^s d\tau \mathcal{M}_i^T \mathcal{M}_i + \epsilon \mathbf{I}) \cdot \mathbf{k}]$ where \mathbf{I} is the 2×2 unit matrix. By exchanging the order of the \mathbf{k} and s integrals, we perform the Gaussian integral for \mathbf{k} and obtain

$$C_{\pi\pi} = \frac{T}{4\pi\Gamma} \int_0^\infty ds F_i(s), \quad (13)$$

$$F_i(s) \equiv \det\left(\int_0^s d\tau \mathcal{M}_i^T \mathcal{M}_i + \epsilon \mathbf{I}\right)^{-1/2}. \quad (14)$$

Then, the behavior of Eq. (13) is determined from that of $F_i(s)$, and thus comes from that of $\mathcal{M}_i(\tau)$.

Let us see how $\mathcal{M}_i(\tau)$ changes in the flow patterns. For the rotational flow $A > S$, it is calculated as [54]

$$\mathcal{M}_r(\tau) = \begin{pmatrix} \cos(\tau\Omega_r/2) & \frac{S-A}{\Omega_r} \sin(\tau\Omega_r/2) \\ \frac{S+A}{\Omega_r} \sin(\tau\Omega_r/2) & \cos(\tau\Omega_r/2) \end{pmatrix}, \quad (15)$$

where $\Omega_r = \sqrt{A^2 - S^2}$. For the elongational flow $S > A$, the frequency Ω_r turns to the imaginary one $i\Omega_e = i\sqrt{S^2 - A^2}$ and the trigonometric functions also turn to the hyperbolic functions. Then, we get

$$\mathcal{M}_e(\tau) = \begin{pmatrix} \cosh(\tau\Omega_e/2) & \frac{S-A}{\Omega_e} \sinh(\tau\Omega_e/2) \\ \frac{S+A}{\Omega_e} \sinh(\tau\Omega_e/2) & \cosh(\tau\Omega_e/2) \end{pmatrix}. \quad (16)$$

For the shear flow $A = S$, Ω_r goes to zero and \mathcal{M}_r turns to

$$\mathcal{M}_s(\tau) = \begin{pmatrix} 1 & 0 \\ \tau S & 1 \end{pmatrix}. \quad (17)$$

Therefore, the behaviors of $\mathcal{M}_i(\tau)$ significantly differ in the flow patterns.

Whether $C_{\pi\pi}$ has the IR divergence or not is given as the convergence of the integral of Eq. (13). The convergence is

determined by the tail behaviors of $F_i(s)$ in $s \rightarrow \infty$ which are calculated as [55]

$$F_r(s) \sim s^{-1}, \quad F_e(s) \sim e^{-s\Omega_e/2}, \quad F_s(s) \sim s^{-2}. \quad (18)$$

Therefore, the s -integrals of $F_e(s)$ and $F_s(s)$ converge whereas that of $F_r(s)$ logarithmically diverges due to the slowest tail. Recalling Eqs. (13) and (7), we find that the ordered state is stable even against the NG mode fluctuation under the shear and elongational flows.

Phase diagram.— From Eqs. (13) and (7), we get the expression of the transition point $r^* = -gT/(4\pi\Gamma) \int_0^\infty ds F_i(s)$. By numerically performing s -integral, we obtain the phase boundary $r^*(S, A)$ in the (r, S, A) space. In Fig. 2-(a), we present the resulting phase diagram in $(r, S/A)$ space at $A = 1$. The green (white) region shows the ordered (disordered) phase. We have set the parameters as $g = \Gamma = T = 1$ and $\epsilon = 10^{-3}$. In the $S/A > 1$ region, r^* monotonically increases as S/A increase. In contrast, when we step into the $S/A < 1$ region, r^* diverges to $-\infty$ and the ordered phase disappears.

In Fig. 2 (b)-(d), we plot the onsets of the order parameter below r^* . Figure 2-(b) shows the order parameter Eq. (4) as a function of S/A at $A = 1$ and $r = -1$. The order parameter jumps with a finite gap at $S/A = 1$; namely, it is the first-order transition. However, it turns to the second order transition at $r = r^*$ as shown in Fig. 2-(c). We can derive the onset behavior $\bar{\phi}_R \propto (S/A - 1)^{1/4}$ by expanding $F_e(s)$ at $s \rightarrow \infty$ in $\delta = S/A - 1$ [56]. Furthermore, Fig. 2-(d) plots the order parameter as a function of r at $S = 1.5$ and $A = 1$, where the second-order transition occurs. In Eq. (4), $C_{\pi\pi}$ is independent of r and then $\bar{\phi}_R^2$ is linear in r for $r < r^*$ and zero at $r = r^*$. Therefore, we have the onset behavior of Fig. 2-(d). In summary, the solid and dotted boundaries of Fig. 2-(a) represent the second- and first-order transitions, respectively. The critical exponents are given as $\bar{\phi}_R \propto |r - r_c|^{1/2}$ on the solid line and $\bar{\phi}_R \propto (S/A - 1)^{1/4}$ at the endpoint.

Discussion.— We discuss the mechanism of how the IR divergence is suppressed. The key to understanding is the advected wavenumber $\mathbf{q}(t)$. The infinite growth of $\mathbf{q}(t)$ at $t \rightarrow \infty$ masks the low- \mathbf{k} behavior of the equilibrium.

We first note that the IR divergence of the equilibrium system comes from the low- $|\mathbf{k}|$ behavior of the diffusion. The correlation function Eq. (11) at $S = A = 0$ is of the equilibrium. Then, $\mathbf{q}(\tau/2)$ returns to \mathbf{k} and the shoulder of the exponential turns to $-s\Gamma \mathbf{k}^2$ which is of the diffusion mode. Thus, we get the familiar result $C_{\pi\pi} = T/(2\pi\Gamma) \int_{2\pi/L}^{\Lambda_{UV}} dk k^{-2} \sim \log(L\Lambda_{UV})$ where k is $|\mathbf{k}|$ and Λ_{UV} is the UV cutoff. $C_{\pi\pi}$ diverges in the limits $L \rightarrow \infty$ and $\Lambda_{UV} \rightarrow \infty$, which are the IR and the UV divergences, respectively. Therefore, the IR divergence comes from the low- k behavior of diffusion.

Under the linear flows, \mathbf{k} is replaced by $\mathbf{q}(\tau/2)$. Then, the behaviors of $\mathbf{q}(\tau)^2$ in $\tau \rightarrow \infty$ determine the IR divergence of $C_{\pi\pi}$. We note that the tail behaviors of Eq. (18) come from $\mathbf{q}(\tau)^2$ in $\tau \rightarrow \infty$. For the rotational flow $A > S$, $\mathbf{q}(\tau/2)^2$ oscillates with the frequency Ω_r in τ as seen from Eq. (15). In contrast, for the elongational flow $S > A$, the hyperbolic

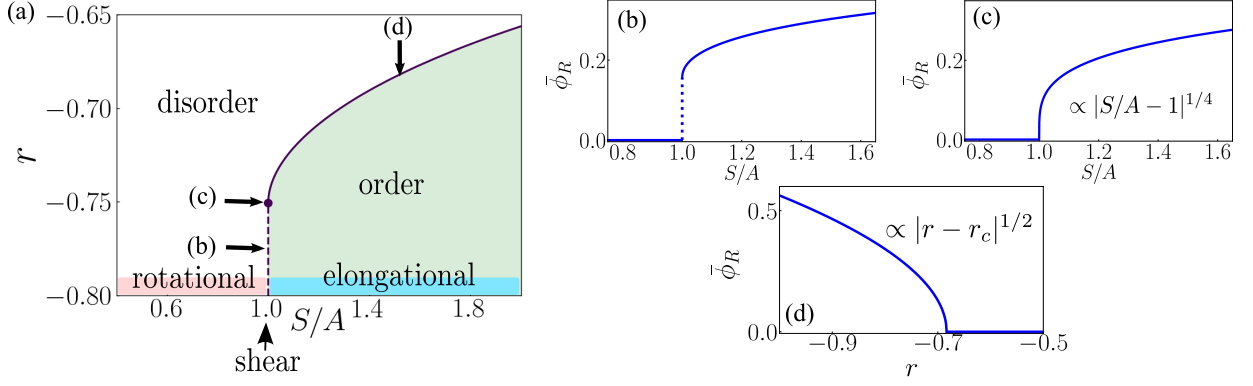


FIG. 2. (a): Phase diagram in $(r, S/A)$ space at $A = 1$. The ordered phase lies on the region $S/A \geq 1$, corresponding shear and elongational flow. (b), (c) and (d): Order parameter as a function of S/A in (b) and (c), and of r in (d). The crossing ways of (b), (c), and (d) to the boundary are shown in Fig. (a).

functions of Eq. (16) gives the exponential growth $q(\tau/2)^2 \sim e^{\tau\Omega_e}$ in $\tau \rightarrow \infty$. For the shear flow $S = A$, we have $q(\tau/2)^2 \sim \tau^2$ from Eq. (17) and it algebraically growth in τ . Therefore, $q(\tau)^2$ diverges in $\tau \rightarrow \infty$ for the elongational and the shear flows. These divergent growths mask the low- k behavior of the diffusion and suppress the IR divergence.

We can also see the connection between the divergent growth of $q(t)$ and the suppression of the fluctuation from the dynamics. The average motion of π^α is given by [57]

$$\langle \pi^\alpha(t, \mathbf{k}) \rangle = \exp \left[-\Gamma \int_0^t d\tau q(\tau)^2 \right] \pi^\alpha(t=0, \mathbf{q}(t)), \quad (19)$$

where $\pi^\alpha(t=0, \mathbf{q}(\tau))$ is the advected initial state: $\pi^\alpha(t=0, \mathbf{q}(t)) = e^{t(\mathcal{D}^T \cdot \mathbf{k}) \cdot \nabla_{\mathbf{k}}} \pi^\alpha(t=0, \mathbf{k})$. Therefore, the average of $\pi^\alpha(t, \mathbf{k})$ diffuses with $\mathbf{q}(\tau)$ and the divergent growth of $q(\tau)^2$ means faster decay of the fluctuation.

The next question is what is the physical meaning of $q(\tau)$. From the definition (10), it is the solution of the advection motion described by $\partial_t \mathbf{q}(t) = (\mathcal{D}^T \cdot \mathbf{k}) \cdot \nabla_{\mathbf{k}} \mathbf{q}(t)$, with the initial value $\mathbf{q}(0) = \mathbf{k}$. Thus, $\mathbf{q}(\tau)$ is the wavenumber advected by the flow $\tilde{\mathbf{v}}(\mathbf{k}) = \mathcal{D}^T \cdot \mathbf{k}$. Figure 3 shows the time evolution of $\mathbf{q}(t)$. The magenta arrows plots $\mathbf{q}(t)$ at several times. The dark- and light-blue lines are the streamlines of $\tilde{\mathbf{v}}(\mathbf{k})$ and the line passing through $\mathbf{q}(t=0)$, respectively. Figure 3-(a) shows $\mathbf{q}(t)$ under the rotational flow. The initial vector $\mathbf{q}(0)$ is just rotated along the rotational flow and its magnitude oscillates in time. Figure 3-(b) shows $\mathbf{q}(t)$ under the elongational flow. $\mathbf{q}(0)$ is advected to the outgoing direction and its magnitude is being stretched. Figure 3-(c) shows $\mathbf{q}(t)$ under the shear flow. $\mathbf{q}(0)$ is stretched along the streamline as well. The flow direction of $\tilde{\mathbf{v}}(\mathbf{k}) = \mathcal{D}^T \cdot \mathbf{k}$ is transposed from $\mathbf{v}(\mathbf{x}) = \mathcal{D} \cdot \mathbf{x}$.

In conclusion, the shear and elongational flows stretch the magnitude of the wavenumber and mask the low-wavenumber behavior of the diffusion. The rotational flow periodically deforms the wavenumber and cannot suppress the IR divergence.

Concluding remarks.— In the flocking hydrodynamics, the advective nonlinear interaction stabilizes the order [5–7, 19].

The mechanisms of the advection are different from our model but its importance is common. Therefore, it is interesting to study the relation to the self-advection of active matter. Of particular interest is the relation between the stretching of the advected wavenumber and the stretching of fluctuations by the anomalous diffusion in the active matter [29]. It will lead to a deep understanding of the origin of the 2D LROs from a more

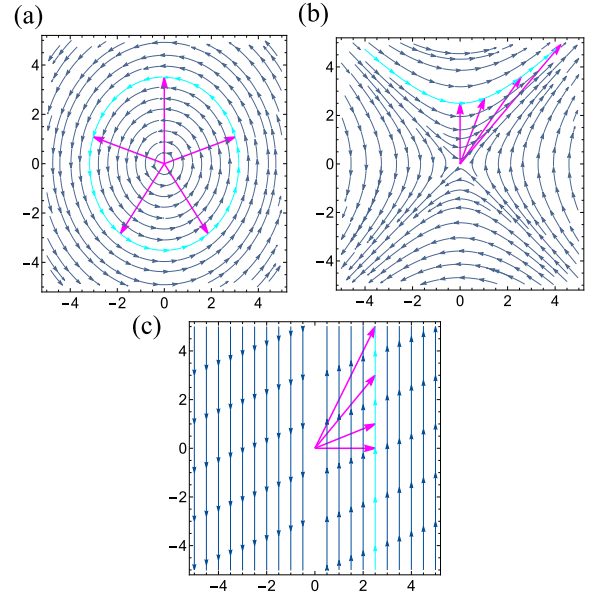


FIG. 3. Time evolution of the advected wavenumber $\mathbf{q}(t)$. The magenta arrows show $\mathbf{q}(t)$ at several times. The dark- and light-blue lines show the stream-lines of $\tilde{\mathbf{v}}(\mathbf{k}) = \mathcal{D}^T \cdot \mathbf{k}$ and the line passing through $\mathbf{q}(0)$, respectively. (a): $\mathbf{q}(t)$ under the rotational flow with $S = 0.1$ and $A = 1.0$. (b): $\mathbf{q}(t)$ under the elongational flow with $S = 1$ and $A = 0$. (c): shows $\mathbf{q}(t)$ under the shear flow with $S = A = 0.2$. The initial vectors of (a), (b), and (c) are $\mathbf{q}(0) = (0, 3.5)$, $(0, 2.5)$, and $(2.5, 0)$, respectively.

general perspective. However, we leave it as future work.

Fluctuations generally tend to be suppressed in the large- N limit and become larger at finite N . However, we expect the ordered state of our model is not broken even at finite N . We note that the LRO under the shear flow at $N = 2$ has been established by the finite size scaling analysis [34]. In addition, the stretching effect of the elongational flow is much stronger than the shear flow whereas the rotational flow cannot stabilize even in the large- N limit. Therefore, our results will be qualitatively valid at finite N .

We finally remark on relations to experiments. We expect our setup to be realized in synchronization transition of a chemical oscillation reaction [58, 59]. In a uniform oscillation of the synchronization transition, $U(1)$ phase symmetry is spontaneously broken. A chemical reaction solution is a fluid and then we can realize the steady flows. In particular, the 2D elongational flow has been recently realized in the experiment [60]. Therefore, we expect that the uniform oscillation under the rotational flow becomes inhomogeneous as the system size increases whereas it sustains under the shear and the elongational flows.

Acknowledgement.— We are grateful to Keiji Saito and Yoshimasa Hidaka for the valuable discussions. This work is supported by JSPS KAKENHI (Grant Numbers JP19H05791, JP21J00034, and JP22K13978)

-
- [1] N. D. Mermin, Phys. Rev. **176**, 250 (1968).
 - [2] P. C. Hohenberg, Phys. Rev. **158**, 383 (1967).
 - [3] N. D. Mermin and H. Wagner, Phys. Rev. Lett. **17**, 1133 (1966).
 - [4] T. Vicsek, A. Czirók, E. Ben-Jacob, I. Cohen, and O. Shochet, Phys. Rev. Lett. **75**, 1226 (1995).
 - [5] J. Toner and Y. Tu, Physical review letters **75**, 4326 (1995).
 - [6] J. Toner and Y. Tu, Physical review E **58**, 4828 (1998).
 - [7] J. Toner, Physical Review E **86**, 031918 (2012).
 - [8] C. A. Weber, T. Hanke, J. Deseigne, S. Léonard, O. Dauchot, E. Frey, and H. Chaté, Phys. Rev. Lett. **110**, 208001 (2013).
 - [9] N. Kumar, H. Soni, S. Ramaswamy, and A. Sood, Nature communications **5**, 4688 (2014).
 - [10] D. Nishiguchi, K. H. Nagai, H. Chaté, and M. Sano, Phys. Rev. E **95**, 020601 (2017).
 - [11] H. Soni, N. Kumar, J. Nambisan, R. K. Gupta, A. Sood, and S. Ramaswamy, Soft Matter **16**, 7210 (2020).
 - [12] J. Iwasawa, D. Nishiguchi, and M. Sano, Phys. Rev. Research **3**, 043104 (2021).
 - [13] S. Zhou, A. Sokolov, O. D. Lavrentovich, and I. S. Aranson, Proceedings of the National Academy of Sciences **111**, 1265 (2014).
 - [14] F. Ginelli, F. Peruani, M. Bär, and H. Chaté, Phys. Rev. Lett. **104**, 184502 (2010).
 - [15] B. Mahault, F. Ginelli, and H. Chaté, Phys. Rev. Lett. **123**, 218001 (2019).
 - [16] B. Mahault and H. Chaté, Phys. Rev. Lett. **127**, 048003 (2021).
 - [17] J. Toner, Phys. Rev. Lett. **108**, 088102 (2012).
 - [18] S. L. Bore, M. Schindler, K.-D. N. T. Lam, E. Bertin, and O. Dauchot, Journal of Statistical Mechanics: Theory and Experiment **2016**, 033305 (2016).
 - [19] L. P. Dadhichi, A. Maitra, and S. Ramaswamy, Journal of Statistical Mechanics: Theory and Experiment **2018**, 123201 (2018).
 - [20] M. Capiulis, M. Tarzia, L. F. Cugliandolo, and O. Dauchot, Journal of Statistical Mechanics: Theory and Experiment **2020**, 013209 (2020).
 - [21] M. Capiulis, M. Tarzia, L. F. Cugliandolo, and O. Dauchot, Physical Review Letters **124**, 198001 (2020).
 - [22] A. Maitra, P. Srivastava, M. C. Marchetti, S. Ramaswamy, and M. Lenz, Phys. Rev. Lett. **124**, 028002 (2020).
 - [23] H. Tasaki, Phys. Rev. Lett. **125**, 220601 (2020).
 - [24] J. Toner, N. Guttenberg, and Y. Tu, Phys. Rev. Lett. **121**, 248002 (2018).
 - [25] R. Das, M. Kumar, and S. Mishra, Phys. Rev. E **98**, 060602 (2018).
 - [26] N. Sarkar, A. Basu, and J. Toner, Phys. Rev. E **104**, 064611 (2021).
 - [27] L. P. Dadhichi, J. Kethapelli, R. Chajwa, S. Ramaswamy, and A. Maitra, Phys. Rev. E **101**, 052601 (2020).
 - [28] S. A. Loos, S. H. Klapp, and T. Martynec, arXiv:2206.10519 (2022).
 - [29] F. Ginelli, The European Physical Journal Special Topics **225**, 2099 (2016).
 - [30] H. Chaté, Annual Review of Condensed Matter Physics **11**, 189 (2020).
 - [31] P. G. D. Gennes, Molecular Crystals and Liquid Crystals **34**, 91 (1976).
 - [32] F. Corberi, G. Gonnella, E. Lippiello, and M. Zannetti, Journal of Physics A: Mathematical and General **36**, 4729 (2003).
 - [33] Y. Minami, H. Nakano, and Y. Hidaka, Phys. Rev. Lett. **126**, 141601 (2021).
 - [34] H. Nakano, Y. Minami, and S.-i. Sasa, Phys. Rev. Lett. **126**, 160604 (2021).
 - [35] H. Nakano, Y. Minami, T. Haga, and S.-i. Sasa, arXiv preprint arXiv:2107.13183 (2021).
 - [36] K. E. Bassler and Z. Rácz, Phys. Rev. E **52**, R9 (1995).
 - [37] U. C. Täuber, V. K. Akkineni, and J. E. Santos, Phys. Rev. Lett. **88**, 045702 (2002).
 - [38] M. D. Reichl, C. I. Del Genio, and K. E. Bassler, Phys. Rev. E **82**, 040102 (2010).
 - [39] Y. Nambu and G. Jona-Lasinio, Phys. Rev. **122**, 345 (1961).
 - [40] J. Goldstone, Il Nuovo Cimento (1955-1965) **19**, 154 (1961).
 - [41] J. Goldstone, A. Salam, and S. Weinberg, Phys. Rev. **127**, 965 (1962).
 - [42] Y. Minami and Y. Hidaka, Physical Review E **97**, 012130 (2018).
 - [43] Y. Hidaka and Y. Minami, Progress of Theoretical and Experimental Physics **2020**, 033A01 (2020).
 - [44] M. Hongo, S. Kim, T. Noumi, and A. Ota, Physical Review D **103**, 056020 (2021).
 - [45] P. M. Chaikin, T. C. Lubensky, and T. A. Witten, *Principles of condensed matter physics*, Vol. 10 (Cambridge university press Cambridge, 1995).
 - [46] A. Onuki and K. Kawasaki, Progress of Theoretical Physics **63**, 122 (1980).
 - [47] A. Onuki and K. Kawasaki, Progress of Theoretical Physics Supplement **69**, 146 (1980).
 - [48] A. Onuki, *Phase transition dynamics* (Cambridge University Press, 2002).
 - [49] See Supplemental Material for correlation functions in the $1/N$ expansion.
 - [50] We can show that the advective term $\mathbf{k} \cdot \mathcal{D} \cdot \nabla_{\mathbf{k}}$ does not lead to singularity in $\mathbf{k} \rightarrow \mathbf{0}$ and r_R is the remaining term by using Eq. (9).
 - [51] See Supplemental Material for derivation of the operator decomposition Eq. (9).

- [52] See Supplemental Material for the average motion of the fluctuation π^a .
- [53] See the discussion for the details.
- [54] See Supplemental Material for calculation of $\mathcal{M}_i(\tau)$.
- [55] See Supplemental Material for the explicit expressions and the plots of $F_i(s)$.
- [56] See Supplemental Material for scaling behavior in Fig. 2-(c).
- [57] See Supplemental Material.
- [58] Y. Kuramoto, *Chemical Oscillations, Waves, and Turbulence*, Dover Books on Chemistry Series (Dover Publications, 2003).
- [59] R. Toth, A. F. Taylor, and M. R. Tinsley, *The Journal of Physical Chemistry B* **110**, 10170 (2006).
- [60] S. Varchanis, S. J. Haward, C. C. Hopkins, A. Syrakos, A. Q. Shen, Y. Dimakopoulos, and J. Tsamopoulos, *Proceedings of the National Academy of Sciences* **117**, 12611 (2020), <https://www.pnas.org/doi/pdf/10.1073/pnas.1922242117>.

Supplemental Material for “Origin of long-range order in a two-dimensional nonequilibrium system under laminar flows”

Yuki Minami¹ and Hiroyoshi Nakano²

¹*Department of Physics, Keio University, Kanagawa 223-8522, Japan*

²*Department of Applied Physics and Physico-Informatics, Keio University, Kanagawa 223-8522, Japan*

CORRELATION FUNCTIONS IN THE $1/N$ EXPANSION

We derive Eqs. (4), (5) and (6). For later convenience, we recast the equation of motion Eq. (2) into the form

$$\frac{\partial}{\partial t}\phi^a = -\Gamma\left[\chi_0^{-1} + \frac{g}{N} \sum_b (\phi^b)^2\right]\phi^a + \eta^a, \quad (\text{S1})$$

$$\chi_0^{-1} = \mathbf{x} \cdot \frac{\mathcal{D}^T}{\Gamma} \cdot \nabla - \nabla^2 + r. \quad (\text{S2})$$

We consider the fluctuations $\sigma(t, \mathbf{x})$ and $\pi^\alpha(t, \mathbf{x})$ from $\bar{\phi}_R$ in the ordered state:

$$\phi^a(t, \mathbf{x}) = (\sqrt{N}\bar{\phi}_R + \sigma(t, \mathbf{x}), \pi^\alpha(t, \mathbf{x})), \quad (\text{S3})$$

where $\alpha = 2, 3, \dots, N$. Substituting Eq. (S3) into Eq. (S1), we obtain

$$\begin{aligned} \left[\frac{1}{\Gamma} \frac{\partial}{\partial t} + \chi_0^{-1} + 3g\bar{\phi}_R^2 + \frac{g}{N} \left(\sum_\alpha (\pi^\alpha)^2 + \sigma^2 \right) \right] \sigma \\ + \sqrt{N}\bar{\phi}_R \left[r + g\bar{\phi}_R^2 + \frac{g}{N} \left(\sum_\alpha (\pi^\alpha)^2 + 3\sigma^2 \right) \right] = \frac{\eta^1}{\Gamma}, \end{aligned} \quad (\text{S4})$$

$$\left[\frac{1}{\Gamma} \frac{\partial}{\partial t} + \chi_0^{-1} + g\bar{\phi}_R^2 + \frac{g}{N} \left(\sum_\alpha (\pi^\alpha)^2 + \sigma^2 + 2\sqrt{N}\bar{\phi}_R\sigma \right) \right] \pi^\beta = \frac{\eta^\beta}{\Gamma}. \quad (\text{S5})$$

We calculate the correlation functions in $1/N$ expansion and thus counting N is important. We note that π^α correlation yields the factor $N - 1$ as

$$\sum_\alpha \langle (\pi^\alpha)^2 \rangle = (N - 1) \langle (\pi^\beta)^2 \rangle, \quad (\text{S6})$$

where π^β is an arbitrary component and equivalent to the other thanks to the $O(N - 1)$ symmetry. In contrast, $\langle \sigma^2 \rangle$ is one component and does not yield the factor N .

Then, for the leading order calculation, we can replace the nonlinear term by

$$\frac{1}{N} \left(\sum_\alpha (\pi^\alpha)^2 + \sigma^2 \right) \sim \langle (\pi^\beta)^2 \rangle, \quad (\text{S7})$$

$$\equiv C_{\pi\pi}, \quad (\text{S8})$$

and obtain

$$\left[\frac{1}{\Gamma} \frac{\partial}{\partial t} + \chi_0^{-1} + 3g\bar{\phi}_R^2 + gC_{\pi\pi} \right] \sigma + \sqrt{N}\bar{\phi}_R \left[r + g(\bar{\phi}_R^2 + C_{\pi\pi}) \right] = \frac{\eta^1}{\Gamma}, \quad (\text{S9})$$

$$\left[\frac{1}{\Gamma} \frac{\partial}{\partial t} + \chi_0^{-1} + g(\bar{\phi}_R^2 + C_{\pi\pi}) \right] \pi^\beta = \frac{\eta^\beta}{\Gamma}, \quad (\text{S10})$$

where we have discarded the sub-leading terms in $1/N$.

We first derive Eq. (4) for $\bar{\phi}_R$. Taking the noise average of Eq. (S9), we have

$$\bar{\phi}_R \left[r + g(\bar{\phi}_R^2 + C_{\pi\pi}) \right] = 0. \quad (\text{S11})$$

Therefore, we obtain Eq. (4) as $\bar{\phi}_R \neq 0$. In addition, by Eq. (4), Eqs. (S9) and (S10) turn to

$$\left[\frac{\partial}{\partial t} + \mathbf{x} \cdot \mathcal{D} \cdot \nabla - \Gamma \left(\nabla^2 - 2r - 2gC_{\pi\pi} \right) \right] \sigma(t, \mathbf{x}) = \eta^1(t, \mathbf{x}), \quad (\text{S12})$$

$$\left[\frac{\partial}{\partial t} + \mathbf{x} \cdot \mathcal{D} \cdot \nabla - \Gamma \nabla^2 \right] \pi^\beta(t, \mathbf{x}) = \eta^\beta(t, \mathbf{x}). \quad (\text{S13})$$

We perform the Fourier transform on the space

$$\left[\frac{\partial}{\partial t} - \mathbf{k} \cdot \mathcal{D} \cdot \nabla_{\mathbf{k}} + \Gamma \left(\mathbf{k}^2 + 2r + 2gC_{\pi\pi} \right) \right] \sigma(t, \mathbf{k}) = \eta^1(t, \mathbf{k}), \quad (\text{S14})$$

$$\left[\frac{\partial}{\partial t} - \mathbf{k} \cdot \mathcal{D} \cdot \nabla_{\mathbf{k}} + \Gamma \mathbf{k}^2 \right] \pi^\beta(t, \mathbf{k}) = \eta^\beta(t, \mathbf{k}). \quad (\text{S15})$$

By multiplying Eq. (S14) by $\sigma(t, -\mathbf{k})$ and taking the noise average, we obtain

$$\left[\frac{1}{2} \frac{\partial}{\partial t} - \frac{1}{2} \mathbf{k} \cdot \mathcal{D} \cdot \nabla_{\mathbf{k}} + \Gamma \left(\mathbf{k}^2 + 2r + 2gC_{\pi\pi} \right) \right] \langle \sigma(t, \mathbf{k}) \sigma(t, -\mathbf{k}) \rangle = T, \quad (\text{S16})$$

where we have used $\langle \eta^1(t, \mathbf{k}) \sigma(t, -\mathbf{k}) \rangle = T$. We can drop the time derivative term for the steady state at $t \rightarrow \infty$, and get

$$\langle \sigma(\mathbf{k}) \sigma(-\mathbf{k}) \rangle = \frac{T}{-(1/2) \mathbf{k} \cdot \mathcal{D} \cdot \nabla_{\mathbf{k}} + \Gamma \left(\mathbf{k}^2 + 2r + 2gC_{\pi\pi} \right)}, \quad (\text{S17})$$

By returning to the real space, we arrive at

$$\langle \sigma(\mathbf{x})^2 \rangle = \int \frac{d\mathbf{k}}{(2\pi)^2} \frac{T\Gamma}{\mathbf{k}^2 - (1/2\Gamma) \mathbf{k} \cdot \mathcal{D} \cdot \nabla_{\mathbf{k}} - 2(r + gC_{\pi\pi})}. \quad (\text{S18})$$

We also obtain $C_{\pi\pi} = \langle \pi(\mathbf{x})^2 \rangle$ which is Eq. (6) by repeating the same calculation for Eq. (S15).

DERIVATION OF THE OPERATOR DECOMPOSITION EQ. (9)

We consider the time-evolution operator

$$U_I(t) = e^{tH_I + tH_0} e^{-tH_0}, \quad (\text{S19})$$

which is in the interaction representation based on the reference frame of H_0 . H_0 and H_I are given by

$$H_0 = \frac{1}{2} (\mathcal{D}^T \cdot \mathbf{k}) \cdot \nabla_{\mathbf{k}}, \quad (\text{S20})$$

$$H_I = -\Gamma \mathbf{k}^2. \quad (\text{S21})$$

The time derivative of $U_I(t)$ is calculated as follows

$$\frac{\partial U_I(t)}{\partial t} = e^{tH_I + tH_0} (H_I + H_0 - H_0) e^{-tH_0}, \quad (\text{S22})$$

$$= e^{tH_I + tH_0} e^{-tH_0} \left(e^{tH_0} H_I e^{-tH_0} \right), \quad (\text{S23})$$

$$= U_I(t) H_I(t). \quad (\text{S24})$$

where we have introduced $H_I(t) = e^{tH_0} H_I e^{-tH_0}$. We note that the order of $U_I(t)$ and $H_I(t)$ in r.h.s is opposite to that in usual quantum mechanics. The formal solution of this equation is given by

$$U_I(t) = \tilde{\mathcal{T}} \exp \left[\int_0^t d\tau H_I(\tau) \right], \quad (\text{S25})$$

where $\tilde{\mathcal{T}}$ is the anti time-ordered product:

$$\tilde{\mathcal{T}} \left[H_I(t_1) H_I(t_2) \right] = \begin{cases} H_I(t_1) H_I(t_2) & \text{for } t_1 < t_2, \\ H_I(t_2) H_I(t_1) & \text{for } t_1 > t_2. \end{cases} \quad (\text{S26})$$

We then calculate $H_I(t)$ as

$$H_I(t) = -\Gamma e^{tH_0} \mathbf{k}^2 e^{-tH_0}, \quad (\text{S27})$$

$$= -\Gamma \mathbf{q}(t/2)^2. \quad (\text{S28})$$

Here, $\mathbf{q}(t/2) \equiv e^{tH_0} \mathbf{k} e^{-tH_0}$ is the advected wavenumber and the factor 1/2 in the argument of \mathbf{q} appears for consistency with the definition Eq. (10). Because $H_I(t)$ is not the operator in the wavenumber space, we can drop $\tilde{\mathcal{T}}$ in Eq. (S25). Therefore, from Eqs. (S19), (S25) and (S28), we have

$$e^{tH_I+tH_0} e^{-tH_0} = \exp\left[-\Gamma \int_0^t d\tau \mathbf{q}(\tau/2)^2\right]. \quad (\text{S29})$$

By multiplying this by e^{tH_0} , we get Eq. (9).

AVERAGE MOTION OF THE FLUCTUATION π^α

By taking the noise average of Eq. (S15), we have

$$\left[\frac{\partial}{\partial t} - \mathbf{k} \cdot \mathcal{D} \cdot \nabla_{\mathbf{k}} + \Gamma \mathbf{k}^2\right] \langle \pi^\beta(t, \mathbf{k}) \rangle = 0, \quad (\text{S30})$$

and the solution is written as

$$\langle \pi^\beta(t, \mathbf{k}) \rangle = \exp\left[t\mathbf{k} \cdot \mathcal{D} \cdot \nabla_{\mathbf{k}} - t\Gamma \mathbf{k}^2\right] \pi^\beta(t=0, \mathbf{k}), \quad (\text{S31})$$

where $\pi^\beta(t=0, \mathbf{k})$ is the given initial state. We regard the exponential part as the time evolution operator and use the interaction representation Eq. (9). Then, we get

$$\langle \pi^\beta(t, \mathbf{k}) \rangle = \exp\left[-\Gamma \int_0^t d\tau \mathbf{q}(\tau)^2\right] \pi^\beta(t=0, \mathbf{q}(\tau)), \quad (\text{S32})$$

where $\pi^\beta(t=0, \mathbf{q}(\tau))$ is the initial state in the interaction representation

$$\pi^\beta(t=0, \mathbf{q}(t)) = \exp\left[t\mathbf{k} \cdot \mathcal{D} \cdot \nabla_{\mathbf{k}}\right] \pi^\beta(t=0, \mathbf{k}). \quad (\text{S33})$$

We note that an arbitrary function of the wavenumber $f(\mathbf{k})$ operated by $e^{t\mathbf{k} \cdot \mathcal{D} \cdot \nabla_{\mathbf{k}}}$ is written as the function of the advected wavenumber

$$\exp\left[t\mathbf{k} \cdot \mathcal{D} \cdot \nabla_{\mathbf{k}}\right] f(\mathbf{k}) = f(\mathbf{q}(t)). \quad (\text{S34})$$

CALCULATION OF $\mathcal{M}_i(\tau)$

We derive Eqs. (15). The eigenvalue λ_\pm and the eigenvector \mathbf{e}_\pm of \mathcal{D}^T are calculated as

$$\lambda_\pm = \pm \sqrt{S^2 - A^2}, \quad (\text{S35})$$

$$\mathbf{e}_\pm = \frac{1}{\sqrt{2S}} \begin{pmatrix} \sqrt{S-A} \\ \pm \sqrt{S+A} \end{pmatrix}, \quad (\text{S36})$$

The eigenvalues λ_\pm are real for the elongational flow ($S > A$) and pure imaginary for the rotational flow ($A > S$), respectively. For the shear flow, they are zero and degenerate. From the eigenvectors, we have the diagonalizing matrix for $S \neq A$

$$P = \frac{1}{\sqrt{2S}} \begin{pmatrix} \sqrt{S-A} & \sqrt{S-A} \\ \sqrt{S+A} & -\sqrt{S+A} \end{pmatrix}. \quad (\text{S37})$$

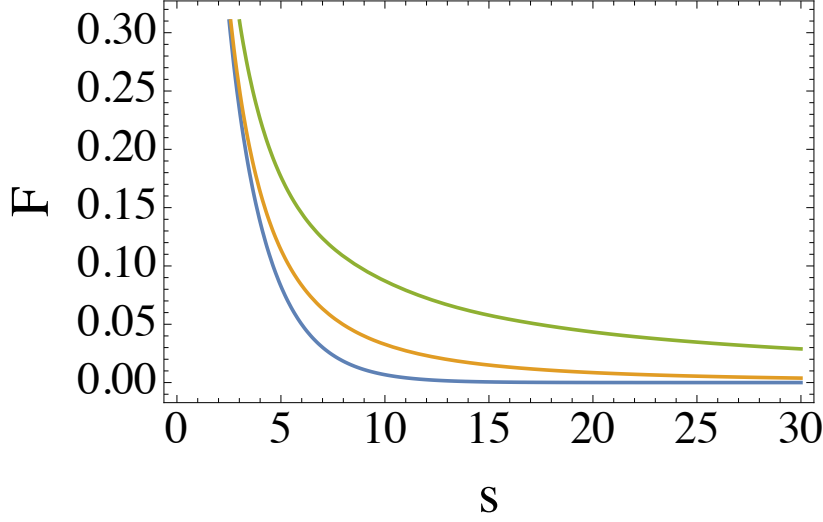


FIG. S1. $F_i(s)$ with several S and A . The blue, orange and green lines show $F_i(s)$ with $(S, A) = (1, 0)$, $(1, 1)$ and $(0.5, 1)$, respectively.

We then calculate $\mathcal{M}_i(\tau) = \exp[\tau \mathcal{D}^T / 2]$ as follows

$$\exp\left(\frac{\tau}{2} \mathcal{D}^T\right) = P P^{-1} \exp\left(\frac{\tau}{2} \mathcal{D}^T\right) P P^{-1}, \quad (\text{S38})$$

$$= P \begin{pmatrix} e^{\tau \lambda_+ / 2} & 0 \\ 0 & e^{\tau \lambda_- / 2} \end{pmatrix} P^{-1}, \quad (\text{S39})$$

$$= \begin{pmatrix} \cosh(\tau \lambda_+ / 2) & \frac{S-A}{\lambda_+} \sinh(\tau \lambda_+ / 2) \\ \frac{S+A}{\lambda_+} \sinh(\tau \lambda_+ / 2) & \cosh(\tau \lambda_+ / 2) \end{pmatrix}. \quad (\text{S40})$$

where we have used $\lambda_+ = -\lambda_-$. By writing λ_+ as $i\Omega_r$, we get Eq. (15).

EXPLICIT EXPRESSIONS AND PLOTS OF $F_i(s)$

The explicit expressions of $F_i(s)$ are calculated as

$$F_r(s) = \left[\frac{2S^2(\cos(\Omega_r s) - 1) + \Omega_r^2 A^2 s^2}{\Omega_r^4} + 2\epsilon \left(s + \frac{sS^2}{\Omega_r^2} - \frac{S^2 \sin(\Omega_r s)}{\Omega_r^3} \right) \right]^{-1/2}, \quad (\text{S41})$$

$$F_e(s) = \left[\frac{2S^2(\cosh(\Omega_e s) - 1) - \Omega_e^2 A^2 s^2}{\Omega_e^4} + 2\epsilon \left(s - \frac{sS^2}{\Omega_e^2} + \frac{S^2 \sinh(\Omega_e s)}{\Omega_e^3} \right) \right]^{-1/2}, \quad (\text{S42})$$

$$F_s(s) = \left[\frac{1}{12} S^2 s^4 + s^2 + \epsilon \left(2s + \frac{1}{3} S^2 s^3 \right) \right]^{-1/2}. \quad (\text{S43})$$

Figure S1 plots $F_i(s)$. The blue, orange and green lines show $F_e(s)$, $F_s(s)$ and $F_r(s)$, respectively. $F_r(s)$ has the slowest decay among them.

We also argue the UV divergence which occurs in $\epsilon \rightarrow 0$. The leading term of $F_i(s)$ in the limit $s \rightarrow 0$ and the integral of that is calculated as

$$F_i(s) \propto \frac{1}{\sqrt{2\epsilon s}}, \quad (\text{S44})$$

$$\int_0^{\Lambda_0} ds F_i(s) \propto \sqrt{\frac{\Lambda_0}{2\epsilon}}. \quad (\text{S45})$$

where Λ_0 is the upper limit for the asymptotic behavior of $F_i(s)$. This behavior is common among the three flows. The integral diverges in the limit $\epsilon \rightarrow 0$ and thus it is the UV one that we have regulated. In conclusion, the UV divergence appears from the behavior in $s \rightarrow 0$.

SCALING BEHAVIOR IN FIG. 2-(C)

We derive the scaling behavior $\bar{\phi}_R \sim \delta^{1/4}$ with $\delta \equiv S/A - 1$ in Fig. 2-(c). From Eqs.(4) and (13), we see that the dependence of $\bar{\phi}_R$ on S and A comes from the integral of $F_i(s)$.

The asymptotic behavior of $F_e(s)$ in $s \rightarrow \infty$ and its integral are calculated as

$$F_e(s) = \frac{\Omega_e^2}{\sqrt{2}S} e^{-s\Omega_e/2}, \quad (\text{S46})$$

$$\int_{\Lambda_1}^{\infty} ds F_e(s) = \frac{\sqrt{2}\Omega_e}{S} e^{\Lambda_1\Omega_e/2}, \quad (\text{S47})$$

where Λ_1 is the cutoff for the asymptotic behavior. By expanding the integral in δ , we get the following in the leading order

$$\int_{\Lambda_1}^{\infty} ds F_e(s) = \frac{\sqrt{2}}{S} \delta^{1/2}. \quad (\text{S48})$$

Therefore, we have $\bar{\phi}_R^2 \sim \delta^{1/2}$ and thus get the scaling behavior in Fig. 2-(c).
